[P1]

J. Villanen, J. Ollikainen, O. Kivekäs, and P. Vainikainen, "Coupling element based mobile terminal antenna structures," *IEEE Transactions on Antennas and Propagation*, vol. 54, no. 7, pp. 2142 – 2153, July 2006.

Coupling Element Based Mobile Terminal Antenna Structures

Juha Villanen, Jani Ollikainen, *Member, IEEE*, Outi Kivekäs, and Pertti Vainikainen, *Member, IEEE*

***Abstract*—In this paper, internal low-volume antenna structures for mobile terminals are studied. The work concentrates on the possibilities to reduce the volume of mobile terminal antenna elements by efficiently utilizing the radiation of the currents on the mobile terminal chassis. Essentially nonresonant coupling elements are used to optimally couple to the dominating characteristic wavemodes of the chassis. The antenna structures are tuned to resonance with matching circuits. During the last few years, the approach has achieved growing interest—also among industrial manufacturers of mobile terminals. There exist, however, no systematical feasibility and performance studies of the idea. During the work, two antenna models with very low-volume coupling elements are designed and in total four prototypes are constructed. The simulation and measurement results show that the studied antenna concept is a very promising alternative for traditional antenna technologies. The presented analysis provides useful and novel information for the designs of the future low-profile and low-volume mobile terminal antennas.**

***Index Terms*—Chassis, coupling element, low-volume antenna, mobile terminal antennas, multisystem.**

I. Introduction

ONE of the trends in the mobile communication technology has been to significantly decrease the size of the mobile terminal. The size of an electrically small antenna, however, cannot be decreased arbitrarily without its other important properties being affected [1]–[3]. Recently, the research on mobile terminal antennas has concentrated on internal planar inverted-F antenna (PIFA) type antenna structures. Different miniaturization solutions have been found and antenna elements working in the GSM850/900/1800/1900, UMTS and WLAN operational bands have been reported [4]–[15]. Dielectric resonator antennas for mobile terminal applications have been investigated in [16]–[18].

Both sides of the printed circuit board (PCB) of today's mobile terminal have usually continuous ground layers. In addition, planar metal surfaces are commonly used inside mobile terminals as electromagnetic compatibility (EMC) shields. The amount, size, and locations of the EMC shields can vary from phone to phone. The combination of the ground layers and the metal EMC shieldings form for a mobile terminal in RF currents point-of-view a solid metal chassis, the length of which is typically in the range of 80–140 mm and the thickness a few millimeters. During the last two decades, the effect of the conducting mobile terminal chassis on the whole antenna structure performance has been examined [19], [21]–[27]. The results show that the dominating characteristic wavemodes [28], [29] of the chassis have significant contribution on the combined radiation behavior of the chassis and the antenna element. In [19], [21], it was reported that at 900 MHz in a typical mobile terminal with 10% relative bandwidth ($|S_{11}| \leq -6\,\mathrm{dB}$), the small internal self-resonant antenna element like PIFA radiates only about 10% portion of the total radiated power. The rest of the power is radiated by the half-wave dipole-type current distribution of the chassis. In fact, the presence and usage of the chassis as the primary radiator of the mobile terminal has made the implementation of very low-profile antenna elements possible. The maximum dimensions allowed for an internal mobile terminal antenna element are insufficient for an isolated antenna element to cover, e.g., the operational band of the E-GSM900 system (880–960 MHz) with high efficiency. At 1800 MHz, the contribution of the antenna element currents on the total radiated power is larger than at 900 MHz (≈50%) [19], [21]. The results indicates that especially at around 1 GHz, traditional self-resonant antenna elements of mobile terminals work mainly as matching circuits and coupling elements between the feed of the antenna element and the chassis.

The above-described research results and those presented in [20], [30] suggest that the bandwidth of an antenna-chassis combination can be improved by enhancing the coupling from the antenna element to the dominating characteristic wavemode of the chassis. An efficient coupling to the chassis wavemode requires the electric field maximum of a planar antenna element to be located near the electric field maximum of the chassis. In addition, the electric field strength all around the antenna element should be as high as possible, i.e., the volume of the antenna element should be used efficiently. In this respect, the structure of one of the most commonly used internal self-resonant antenna element, PIFA, is not optimal. Near the shorting pin of the PIFA, the voltage and thus also the electric field strength is low. Also, the requirement of the self-resonance is a limiting factor for an antenna designer for two reasons. First, the space requirements for a self-resonant antenna element are rather high at low frequencies, e.g., at the E-GSM900 band. Some kind of meandering of the antenna element is typically used to reduce the total volume of the antenna element [5]–[10]. Second, owing to the meandering at the lower frequencies, the optimal shaping of the antenna element according to the high-coupling locations of the chassis becomes difficult. Thus, there exists potential for more compact antenna structures, which more efficiently make use of the fundamentals of small antenna ele-

Manuscript received March 15, 2005. This work was supported in part by the Academy of Finland, Emil Aaltonen Foundation, Ulla Tuominen Foundation, Nokia foundation, and in part by the HPY Foundation.

J. Villanen, O. Kivekäs, and P. Vainikainen are with Helsinki University of Technology, IDC, SMARAD, Radio Laboratory, FIN-02150 Espoo, Finland (e-mail: juha.villanen@tkk.fi).

J. Ollikainen is with the Nokia Research Center, Helsinki FIN-00045, Finland.

Digital Object Identifier 10.1109/TAP.2006.877162

ments situated in the vicinity of a mobile terminal chassis. In [19]–[21], a novel idea was presented to address the problem. It was suggested that the size of an internal mobile terminal antenna element could be considerably reduced by replacing the self-resonant antenna element with an essentially nonresonant coupling element that efficiently excites the dominating characteristic wavemodes of the chassis. Separate matching circuitry is then used to tune the coupling element-chassis-combination in resonance. In [4], coupling elements were used to implement an extremely low-volume and low-profile quad-band antenna structure for GSM850/900/1800/1900 mobile terminals. The idea of coupling elements has also achieved interest among commercial mobile terminal manufacturers [31].

According to the aforementioned studies, coupling elements seem to be a very promising solution for implementing low-profile and low-volume mobile terminal antennas. There exist, however, no scientific publications with systematic characterization and analysis of the idea. The purpose of this paper is to present a comprehensive study of the suitability of coupling elements for use in mobile terminals. To demonstrate the multiband operation and potential of coupling elements, four prototype antennas have been designed and constructed. The performances of the designed prototypes are validated with both simulations and measurement in free space and in talk-position. In talk-position, both the effect of the head and hand of the user are considered. For comparison, also the performance of two traditional PIFA type antenna structures is studied with simulations. In the first part of this paper, general design considerations of coupling elements and matching circuits are discussed. Based on an extensive series of three-dimensional (3-D) electromagnetic simulations, guidelines for optimal shaping and placement of coupling elements in the vicinity of a chassis are given. In the second part of the paper, the prototype and reference antennas are presented. This is followed by presentation of the simulation and measurement methods. At the end of the paper, the simulation and measurement are presented, analyzed, and discussed.

II. Design Considerations

The antenna structure studied in this paper consists of three main parts. The first part is the mobile terminal chassis, which is meant to work as the main radiator of the antenna structure. To achieve sufficient impedance bandwidth, e.g., at the operational bands of the E-GSM900 system, the dominant wavemode of the chassis has to be excited somehow. For that purpose, the second part of the antenna structure, a coupling element is used. Impedance matching to the transceiver electronics for the selected frequency is done with the third part of the antenna structure, matching circuitry.

A. General

According to the narrowband analysis of [21], the relative bandwidth of the combination of mobile terminal antenna element and chassis is affected by the unloaded quality factor of the antenna element, the level of coupling between the wavemodes of the antenna element and the chassis, and the difference between the resonant frequencies of the antenna element and the chassis. One of the main problems in mobile terminal antenna engineering is to reduce the antenna element volume while preserving the same relative bandwidth. As a well known rule of thumb, reducing the volume of an electrically small antenna element generally increases the antenna element unloaded quality factor. According to [21], the effect of increased unloaded quality factor, however, can be compensated by increasing coupling between the wavemodes of the antenna element and the chassis. More generally, it can be thought that the chassis represents a piece of a thick single-conductor transmission line having high radiation losses. Such a structure obviously provides a possibility for wideband antenna functionality, if one can efficiently couple power into it. The strongest radiation is obtained at the resonances of the structure, as presented in [21], but as shown in this paper, the chassis radiation is significant also at other frequencies. This is actually one of the principal ideas behind coupling elements. As theoretically shown in [21], large relative bandwidths can be achieved with nonresonant high-Q (low-volume) coupling elements, assuming that strong enough coupling to the dominant wavemode of the chassis is obtained. This result will be demonstrated later in this paper with prototype antennas. For simplicity, we have in the above discussion assumed that the resonant frequencies of the antenna element and the chassis are kept constant.

B. Coupling Elements

Coupling to the chassis wavemode can be done either via the magnetic or the electric fields of the chassis wavemodes [20]. A plate or probe can be arranged so that its electric field direction is parallel to that of the chassis wavemode. Similarly, a loop can be arranged so that its magnetic field coincides with that of the chassis wavemode [20]. This paper concentrates on the possibilities to couple via the electric fields of the chassis, whereas consideration of magnetic coupling is left for future research. The modularity of the structure enables the use of separate coupling elements, e.g., for the up- and downlink bands in frequency duplex radio systems. Furthermore, separate coupling elements can be used to cover, e.g., the E-GSM900 and GSM1800 systems [20]. Since the coupling element does not need to be tuned to resonance, extremely compact coupling elements can be used even at very low frequencies without the need of meandering.

In order to couple strongly to the chassis dominant wavemode, the location and shape of the coupling element have to be chosen correctly. The effect of the coupling element location on the achievable radiation quality factor was studied with IE3D simulator (ver. 10.0) [46]. In the simulations, a small x-axis directed (see Fig. 2. for coordinates) probe with the shape of a circular cylinder was placed at different locations on a $100 \times 40 \times 3\ \mathrm{mm}^3$ $(\mathrm{height} \times \mathrm{width} \times \mathrm{thickness})$ chassis. The height of the probe was 3 mm, and its diameter was 2 mm. An air gap of 0.03 mm was left between the lower end of the probe and the surface of the chassis. The admittance (with 50 Ω termination) seen from a port placed in the air gap between the probe and the chassis was then simulated for each probe location. From the simulated input admittances, radiation quality factors were calculated as the ratio of susceptance to conductance [32]. The

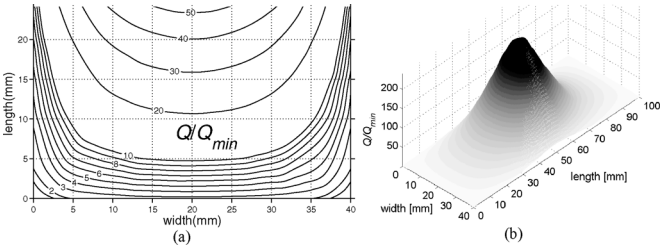

Fig. 1. Normalized ($Q_{\min} = 195$) simulated radiation quality factors at 920 MHz obtained with a small probe moved on top of a chassis with dimensions $100 \times 40 \times 3\ \mathrm{mm}^3$. (a) Closer view on the shorter end of the chassis and (b) 3-D view of the whole chassis.

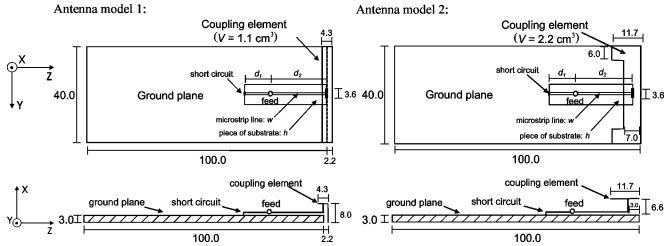

Fig. 2. Geometries of the designed antenna models. d_1 and d_2 denote the longitudinal dimensions of the microstrip lines, $w = \mathrm{microstrip\ line\ width}$ and $h = \mathrm{substrate\ thickness}$. All dimensions are in millimeters.

results were after that normalized to the minimum achieved radiation quality factor ($Q_{\min} = 195$ at the corner of the chassis). Fig. 1 presents the obtained normalized radiation quality factors as a function of the probe location at 920 MHz. The same simulations were also made at 1800 MHz (not graphically presented in this paper). It should be noted that in Fig. 1, low values of normalized radiation quality factors represent the locations where strong coupling to the chassis wavemode has been obtained.

As reported in [21], the shape of a typical mobile terminal chassis current distribution at 900 MHz is similar to that of a half-wave dipole antenna. The electric field maximums are located at the ends of the chassis and the electric field minimum is located at the center of the chassis. This explains the behavior of the curves in Fig. 1. According to Fig. 1, the lowest radiation quality factors can be achieved by placing the coupling element(s) above the corners and shorter ends of the chassis. Very strong coupling was also achieved (not shown in Fig. 1) with a z-axis directed (see Fig. 2.) probe located on the 3 mm thick edges of the chassis. This suggests that in order to achieve the strongest possible coupling to the dominating wavemode of the chassis, the coupling element should additionally be bent over the shorter end of the chassis. As shown in [21], at 900 MHz a standard self-resonant PIFA works mainly as a coupling element. Therefore, at 900 MHz the above described design guidelines should also be valid for traditional self-resonant mobile terminal antenna elements. As shown later in this paper, it is however difficult to efficiently couple with a shorted self-resonant antenna element. At 1800 MHz, the shape of the quality factor curve was similar to that of the 920 MHz curve in Fig. 1. However, the achieved quality factors were larger than at 920 MHz, as can be expected. The lowest order resonant frequency of a 100 mm long chassis is typically close to 1.1 GHz. In consequence, the chassis is almost nonresonant at 1800 MHz, whereas 920 MHz is fairly close to the lowest order resonant frequency of the chassis [19], [21].

C. Matching Circuits

After the coupling element is shaped and located optimally above the chassis, it has to be matched at the correct frequency with a matching circuitry. According to [45], a complex load can be matched perfectly only at a finite number of frequencies. The theoretical maximum obtainable bandwidth is limited by the unloaded quality factor of the complex load, the number of matching resonators, and the applied impedance matching criterion (e.g., $|S_{11}| \leq -6\ \mathrm{dB}$) [45]. In the next two sections, matching circuit topologies and technologies are shortly discussed. Owing to the wide variety of possible matching circuit implementation options, the discussion is presented only at a generic level.

1) Matching Circuit Topologies: Matching of a complex load to single resonance can be done in various ways by using the well-known impedance matching principles [32]. In the simplest case, single-resonant matching circuits are used, but multiresonant and multiband circuit topologies could be used as well, as in [4]. Some examples of single-resonant matching circuit topologies are presented later in this paper in Section V-H. Although different topologies give roughly the same relative bandwidth, some options are more feasible in practice for some specific coupling element. From the lumped element quality factor point of view, for example, topologies that lead to small component values are preferable. Also, the relative tolerances of the used components should be taken into account. One should note, however, that a matching circuit topology being feasible for some specific coupling element might not necessarily be feasible for some another coupling element having, e.g., different dimensions. Therefore, the optimal circuit topology should always be individually tested and chosen for new coupling element-chassis-combinations.

2) Matching Circuit Technologies: The matching circuit components can be implemented using various different distributed or lumped technologies. In this work, for example, microstrip lines have been used to implement the matching circuits for the prototypes. Naturally, also high-Q (low-loss) discrete inductors and capacitors can be used instead of microstrip lines, as in [4]. The advantage of high-Q discrete elements over distributed elements is the significantly lower occupied matching circuit area. Recent advances in integration technology have enabled the implementation of extremely low-volume RF components. Using multilayer low-temperature co-fired ceramic (LTCC) substrates, high-Q inductors, capacitors, transmission lines, and other passive elements can be integrated into a single package having very low volume [33]–[37]. In 2001, an LTCC (14-layer) based triple-band GSM RF front-end module (FOM) integrating more than 40 capacitors and inductors in a package measuring only $6.7 \times 5.5 \times 1.8\ \mathrm{mm}^3$ ($V = 0.07\ \mathrm{cm}^3$) was introduced [33]. Later, a FOM having 60% lower volume than the previous one was published [34]. In [35], detailed design procedures and measurement results were presented for an 8-layer LTCC FOM having similar functionality as [33], [34]. The LTCC substrate volume occupied by, e.g., the combination of an E-GSM900

low-pass filter and an RF choke, consisting of in total three inductors and three capacitors, was only $2 \times 0.8 \times 0.7$ mm^3. The in-band insertion loss was less than 0.3 dB. In [35], further size reduction for the FOM was achieved by replacing the required quarter-wavelength ($\lambda/4$) transmission lines with modified lumped element equivalent circuits. The multilayer LTCC substrate volume occupied by the $\lambda/4$ (at 1800 MHz) transmission line was only $1 \times 1 \times 0.4$ mm^3. The measured insertion loss was less than 0.25 dB below 2 GHz. Based on the above discussed results, it is obvious that by utilizing modern circuit technologies, the matching circuitry for a coupling element can be implemented with high efficiency and within very low circuit board volume. Moreover, integration of the matching circuitry, e.g., within the existing LTCC-based FOM of the mobile terminal should have only minor effects on the production time and costs. One should notice further that in commercial mobile terminals, the RF FOM is typically attached on top of the main PCB as a separate module. In such arrangement, the main PCB volume under the FOM can be utilized for other purposes.

III. Prototype and Reference Antennas

A. Prototype Antennas

To demonstrate the potential of the compact antenna structure studied in this paper, two coupling element-based antenna models were designed with IE3D simulations. Tuning and optimization of the coupling elements were based on the results presented in Section II-B. The target was that both designed coupling elements would satisfy the bandwidth requirements of the E-GSM900 (880–960 MHz) and GSM1800 (1710–1880 MHz) systems. Also radiation efficiencies and specific absorption rates (SARs) beside user's head and hand were considered to be important parameters. To demonstrate the multiband operation of the designed two coupling elements, they were both matched at the E-GSM900 and GSM1800 operating bands with single-resonant matching circuits. In summary, two coupling elements were designed, and in total four prototypes were manufactured. Fig. 2 shows the geometries of the two designed antenna models.

The coupling element of antenna model 1 occupies very low volume, only 1.1 cm^3. The volume of the coupling element of antenna model 2 is 2.2 cm^3. The idea behind antenna model 1 is that the coupling element utilizes its volume optimally by coupling efficiently to the chassis wavemode. This is achieved by bending the coupling element over the shorter end of the chassis. The coupling element of antenna model 2 is placed in a more traditional way, totally above the chassis. To optimize coupling to the chassis wavemode, the shape of the coupling element is chosen to roughly follow the quality factor lines in Fig. 1. The typical dimensions of a mobile terminal chassis, $100 \text{ mm} \times 40 \text{ mm} \times 3 \text{ mm}$ (length $\times$ width $\times$ thickness), were taken for the antenna models. As discussed earlier, chassis dimensions have a significant effect on the bandwidth of an antenna-chassis combination. The optimum length for the chassis with respect to the bandwidth at the E-GSM900 band would be about 130 mm [19], [21]–[23]. Thus, the lengths of the ground planes were not optimized with respect to the bandwidth. The ground planes were made of brass ($\sigma = 2.6 \cdot 10^7$ S/m) and the coupling elements were constructed from a 0.2 mm thick sheet of tin bronze ($\sigma = 0.8 \cdot 10^7$ S/m).

TABLE I
Dimensions of the Microstrip Matching Circuits of the Prototype Antennas. All Dimensions are in Millimetres

	Antenna model 1				Antenna model 2			
System	d_1	d_2	h	w	d_1	d_2	h	w
E-GSM900	11.1	16.7	1.6	1.2	10.9	23.6	1.6	1.2
GSM1800	7.0	0.0	0.8	2.0	7.0	2.0	0.8	2.0

The matching circuits for the prototype antennas were implemented with microstrip lines by photoetching on RT Duroid 5870 ($\sigma = 5.75 \cdot 10^7$ S/m, $\tan\delta = 0.0012$, $\varepsilon_r = 2.33$). The matching circuit modules were then attached on top of the chassis. The general topology of the used matching circuit is shown in Fig. 2 (dimensions d_1, d_2, w, and h). The dimensions of the matching circuits are presented in Table I. One should note that the prototypes have not been optimized in any way with respective to the occupied matching circuit volumes. The microstrip lines could, e.g., be meandered and placed under the coupling elements as in [20], or alternatively, implemented using high-Q discrete lumped elements as in [4]. In real applications, microstrip lines most likely wouldn't be used, since more advanced technologies are available. As discussed in Section II-C, it is obvious that if integrated into the existing LTCC RF front-end module of a modern mobile terminal, the LTCC substrate volumes occupied by the matching circuits of the prototypes would be very low. Since the FOM is typically attached as a separate module on top of the main PCB, the main PCB volume consumption would be practically zero. Furthermore, according to the results presented in [35], the matching circuit losses obtained with the LTCC implementation would most likely be of the same order as with the microstrip lines used in this work. Owing to the aforementioned facts, the volumes occupied by the matching circuits have in this paper been discussed separately from the volumes consumed by the coupling elements.

B. Reference Antennas

For reference, the performance of two traditionally shaped single-band PIFA type antenna structures published in [22] were studied with simulations. The selected two reference antennas have been designed for the E-GSM900 and GSM1800 systems. To obtain simulation results comparable with the designed prototype antennas, the dimensions of the simulation models of the reference antennas were changed as follows. The chassis lengths were changed from 101.05–100 mm, the chassis widths were changed from 41.05–40 mm and the thicknesses were changed from 3.55–3 mm. In addition, the width of the E-GSM900 reference antenna element was changed from 41.05–40 mm. The volumes of the antenna elements of the used E-GSM900 and GSM1800 reference antennas are 5.4 cm^3 and 2.9 cm^3, respectively. The same conductivities for the metal parts of the reference antennas were used as for the prototype antennas.

The antenna elements of the reference antennas are located totally above the chassis (see [22]). In that respect, their performance can be compared to that of antenna model 2, whose

coupling element is also located totally above the chassis. Also, the reference antenna elements are only 0.15 mm lower in height than the coupling element of antenna model 2. Owing to the location and shape of the coupling element of antenna model 1, its performance can be expected to differ from those of the other studied antenna structures.

IV. Simulation and Measurement Methods

To confirm the performance of the designed prototypes, the most important characteristics of a mobile terminal antenna were both simulated and measured. Both free space and talk-position performance of the antenna structures under investigation were evaluated.

A. Simulations and Measurements in Free Space

In free space, the frequency responses of the reflection coefficients, radiation efficiencies, and radiation patterns of the prototype antennas were both simulated and measured. For comparison, the performances of the reference antennas were studied with simulations. The multiband operation of the coupling element of antenna model 2 was further investigated with IE3D simulations over a wide frequency range. The measurements were made in the premises of the Radio Laboratory of Helsinki University of Technology. The free space total and radiation efficiencies of the prototype antennas were computed from the measured (anechoic chamber) 3-D radiation patterns by using the 3-D pattern integration technique [38]. In the results analysis, the widely applied [4], [5], [8], [9], [13], [16], [19]–[23], [26] impedance matching criterion $|S_{11}| \leq -6$ dB has been used to calculate the impedance bandwidths.

Based on the results of [21], it can be expected that the main radiator in the antenna structures studied in this paper at the E-GSM900 band is the dominant wavemode of the chassis. A self-resonant antenna element like PIFAs works in such case mainly as a coupling element [21]. In that respect, the operating principles of the studied E-GSM900 reference PIFA and the coupling elements of the prototypes should be similar. Coupling elements, however, should excite the dominant wavemode of the chassis more efficiently than traditional self-resonant antenna elements, as discussed before. In order to obtain proof for this assumption, simulated (IE3D) chassis current density distributions of the antennas under study were investigated at 920 and 1780 MHz. As shown in [21], the current density distribution of a mobile terminal chassis is a combination of the antenna element currents and the currents of the dipole-type wavemode of the chassis. Therefore, if the current distribution of the dominant wavemode of the chassis is to be studied, the current distributions of the antenna/coupling element and the matching circuitries should somehow be omitted from the results. According to our simulations, the most suitable location for studying the dominant wavemode of the chassis can be found from the backside of the lower end of the chassis (left end of the chassis in Fig. 2), where the currents from other parts of the antenna structure are typically weak. The chassis dominant wavemodes were therefore studied by computing surface integrals of the simulated chassis current densities over the lower halves of the chassis back sides. In order to achieve comparable results, the total radiated powers of the studied antenna structures were normalized to equal by subtracting (in decibels) the simulated total efficiencies from the surface integral results. One should note that the effects of, e.g., the antenna element currents cannot be totally removed from the results. Therefore, the presented results are only indicative.

B. Simulations and Measurements in Talk-Position

In the antenna concept studied in this paper, the chassis is at all frequencies playing a leading role in the total radiation of the mobile terminal. Thus, it can be expected that the influence of the user's head and hand on the performance of a coupling element based antenna structure differs from the user's influence on the performance of more traditional internal mobile terminal antenna structures. To identify these possible performance differences, the talk-position performance of the designed antenna models were studied with measurements and simulations. The same simulations were also made for the reference antennas.

1) Talk-Position Measurements: In the measurements, the SARs of the prototype antennas were analyzed with the DASY4 system [40]. According to the manufacturer of DASY4, the uncertainty of the SAR measurements at 95% probability level is $\pm 20\%$. The prototype under investigation was attached beside the left ear of a head phantom in the standard "cheek" position [39] with the positive x-axis pointing away from the phantom (see Fig. 2. for the coordinate system). The distance between the back side surface of the chassis and the ear of the head phantom was 8 mm, which was assumed to be an average distance between the outer surface of a mobile terminal's plastic cover and the surface of the metal chassis. The loudspeaker location of the phone was assumed 10 mm from the upper end of the chassis. The SARs were measured with the specified mean (rms) output powers of 250 and 125 mW for the E-GSM900 and GSM1800 systems, respectively.

2) Talk-Position Simulations: In the simulations, a commercial SEMCAD simulator [41] was used. The head of the user was modeled with a homogenous specific antropomorphic mannequin (SAM) head model. The material parameter values given in [39] were used for the SAM head model ($\varepsilon_r = 42.0$ and $\sigma = 0.99$ S/m at 900 MHz, $\varepsilon_r = 40.0$ and $\sigma = 1.38$ S/m at 1800 MHz). The antenna structures under investigation were placed beside the left ear of the SAM head model similarly as during the measurements, except that the distance between the back side of the chassis and the ear of the SAM head model was now 7 mm. The hand of the user was modeled with the hand model 2 published in [22]. The used hand model consists of two tissues, bone surrounded by muscle. The material parameters for the bone ($\varepsilon_r = 16.6$ and $\sigma = 0.24$ S/m at 900 MHz, $\varepsilon_r = 15.6$ and $\sigma = 0.43$ S/m at 1800 MHz) and muscle ($\varepsilon_r = 56.0$ and $\sigma = 0.97$ S/m at 900 MHz, $\varepsilon_r = 54.4$ and $\sigma = 1.39$ S/m at 1800 MHz) were the same as used in [22]. The location of the hand model relative to the studied antenna structures was also the same as in [22], i.e., the distance between the upper end of the chassis and the upper edge of the hand model was 30.55 mm. The metal parts of the studied antenna structures were modeled as perfect electric conductors (PEC). For decreasing computation complexity, the microstrip matching circuits were not included in the SEMCAD simulations of antenna model 1 and antenna model 2.

TABLE II
MEASURED IMPEDANCE BANDWIDTHS ($|S_{11}| \leq -6$ dB), BANDWIDTH-TO-VOLUME RATIOS, MAXIMUM DIRECTIVITIES, MAXIMUM REALIZED GAINS, TOTAL AND RADIATION EFFICIENCIES AND SARS FOR THE PROTOTYPE ANTENNAS. THE SAR RESULTS INCLUDE THE EFFECT OF A HEAD PHANTOM. ALL OTHER MEASUREMENTS HAVE BEEN MADE IN FREE SPACE. THE UNCERTAINTY OF THE SAR MEASUREMENTS AT 95% PROBABILITY LEVEL WAS ±20%

	Antenna model 1 (measured)		Antenna model 2 (measured)	
Parameter	**E-GSM900**	**GSM1800**	**E-GSM900**	**GSM1800**
***BW* [MHz]**	873 - 1003	1692 - 1893	880 - 962	1700 - 1915
B_r [%]	13.9	11.2	8.9	11.9
B_r/V-ratio [%/cm^3]	12.6	10.2	4.1	5.4
***D* [dBi]**	3.4 ± 1.2	4.3 ± 1.2	3.3 ± 1.2	4.3 ± 1.2
G_{real} [dBi]	3.1 ± 1.2	4.0 ± 1.2	3.1 ± 1.2	4.0 ± 1.2
η_{tot} [%]	≥ 82 ± 4	≥ 63 ± 4	≥ 74 ± 4	≥ 66 ± 4
η_r [%]	≥ 95 ± 4	≥ 82 ± 4	≥ 94 ± 4	≥ 81 ± 4
SAR_{10g} [W/kg]	1.9	0.8	1.4	0.6
SAR_{max} [W/kg]	3.9	1.8	2.6	1.2

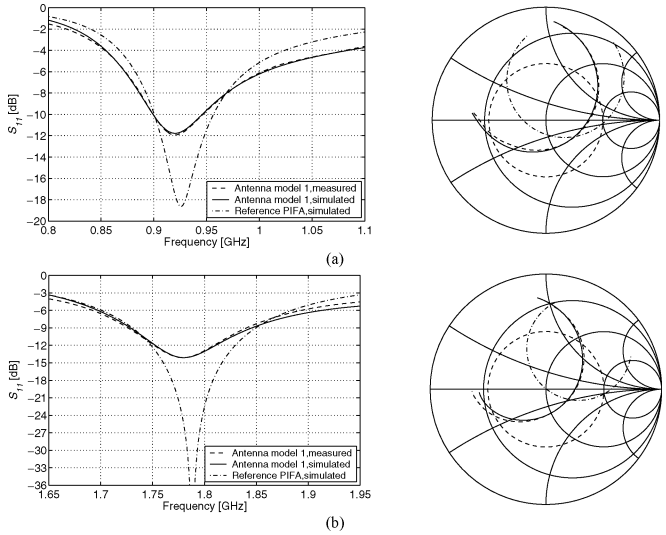

Fig. 3. Simulated (solid line, IE3D) and measured (dashed line) frequency responses of the reflection coefficients for the prototypes of antenna model 1 (a) E-GSM900 prototype and (b) GSM1800 prototype. The dash-dotted lines represent the simulated (IE3D) frequency responses of the reflection coefficients for the E-GSM900 and GSM1800 reference antennas. The dotted circles in the centers of the Smith charts represent $|S_{11}| = -6$ dB.

V. SIMULATION AND MEASUREMENT RESULTS

A. Bandwidth and Coupling Coefficiencts

The simulated and measured frequency responses of the reflections coefficients for the two prototypes of antenna model 1 are presented in Fig. 3. Also, the simulated reflections coefficients for the two reference antennas are presented. From Fig. 3, very good agreement between the simulated and measured results can be observed. The resonant frequencies of the prototype antennas of antenna model 1 are close to those of the reference antennas. The same applies also to the prototypes of antenna model 2 (not shown in Fig. 3). Table II presents the measured absolute (BW) and relative (B_r) impedance bandwidths for all four prototypes. Considering the volume (1.1 cm^3) of the coupling element of antenna model 1, it can be claimed that the obtained relative bandwidths are very high. According to Table II, the prototypes of both antenna models meet the bandwidth requirements of the E-GSM900 and GSM1800 systems.

The obtained relative bandwidth results provide support for the assumption that the studied coupling elements couple more strongly to the dominant wavemode of the chassis than the reference PIFAs. At the E-GSM900 band this can be seen most clearly by comparing the relative bandwidths and antenna/coupling element volumes of antenna model 1 and the reference PIFA. As discussed in Section II-A, the bandwidth of the combination of mobile handset antenna and chassis is mainly determined by the unloaded quality factor of the antenna element and the level of mutual coupling between the wavemodes of the antenna element and the chassis. At the E-GSM900 band, the bandwidth of antenna model 1 is clearly higher than that of the reference PIFA [see Fig. 3(a)]. The coupling element of antenna model 1, however, occupies nearly five times lower volume than the reference antenna element. In order to reach the large relative bandwidth, the coupling element of antenna model 1 therefore has to couple much more strongly than the reference antenna element to the chassis dominant wavemode. The same logic can be used to explain the bandwidth differences between antenna model 1 and antenna model 2.

The logic used above works well also for the bandwidth results obtained at the GSM1800 band. According to Fig. 3(b) and Table II, all studied antenna structures have nearly equal bandwidths at the GSM1800 band. The volume of the reference antenna element, however, is nearly three times as large as the volume of the coupling element of antenna model 1, and roughly 30% larger than the volume of the coupling element of antenna model 2. In order to reach the same bandwidth as the reference antenna structure, the studied coupling elements therefore need to couple more strongly to the dominant wavemode of the chassis than the GSM1800 reference PIFA. The chassis current distribution simulation results analyzed in the next Section will provide more proof for this assumption. In discussion above, we haven't considered the volumes consumed by the matching circuitries of the prototypes. As discussed in Sections II-C and III-A, the substrate volumes consumed by the matching circuitries largely depend on the final implementation technology.

B. Chassis Current Distributions

At 920 MHz, the magnitudes of the surface integrals of the chassis current distributions were almost equal for all the an-

tennas under study, within 0.2 dB from each other. Thus, the powers radiated by the chassis dominant wavemodes seem to be nearly equal. As shown in [21], at 900 a typical internal self-resonant antenna element like PIFA radiates only about 10% portion of the mobile terminal's total radiated power. The same figure for a low-volume coupling element having stronger coupling to the chassis wavemode could intuitively be half less, i.e., 5%. The relative powers radiated by the chassis dominant wavemodes would then be 90% and 95% for the PIFA and coupling element based antenna structures, respectively. The difference between these two values is only 0.2 dB, which considering the uncertainties (see Section IV-A) of the study, is a logical result.

At 1780 MHz, the magnitude of the surface integral of antenna model 2 was roughly 2 dB larger than that of the reference PIFA. Further, the surface integral magnitude of antenna model 1 was roughly 2 dB larger than that of antenna model 2. The results fully support the discussion presented in Sections II-A and V-A. The chassis dominant wavemode currents excited by the coupling elements are clearly stronger than the ones excited by the GSM1800 reference PIFA, as expected. The results also clearly demonstrate the difference between antenna model 1 and antenna model 2. Stronger and more efficient coupling to the dominant wavemode of the chassis is achieved with the coupling element of antenna model 1, as can be expected based on the results of [19], [21].

C. Bandwidth-to-Volume Ratio

For a mobile terminal antenna designer, the extra volume occupied by an antenna structure is one of the most important parameters. With the extra volume, we here denote the additional space required to implement the antenna functionality, excluding the volumes of all the already existing parts of the terminal, like the chassis. In addition to the occupied extra volume, the bandwidth of an antenna structure is one of the key parameters affecting practical antenna design. One way to simultaneously account for both of these parameters is to compute the bandwidth-to-volume ratio for the studied antenna structure. Although representing a somewhat heuristic approach, bandwidth-to-volume ratio can provide useful and practical information for an antenna designer. For instance, consider two mobile terminal antenna structures having roughly the same bandwidths but different volumes. An antenna designer would naturally select the structure consuming less space, i.e., having larger bandwidth-to-volume ratio. The same logic of course also applies for two antenna structures having the same volumes but different bandwidths. An antenna designer obviously also needs to take into account, e.g., SAR issues and all the mechanical constraint affecting antenna design, such as the allowable antenna element height. In this paper, bandwidth-to-volume ratios have been computed as the ratios of the relative bandwidths to the volumes occupied by the antenna or coupling elements. The front-end-module (FOM) substrate volumes occupied by the matching circuitries haven't thus been included in the calculations. As discussed in Sections II-C and III-A, the FOM substrate volumes occupied by the matching circuitries depend largely on the final implementation technology. The circuit technology used in this work was selected only for easy demonstration of the studied antenna concept, and it most likely would not be applied in real mobile terminals. More practical low-volume matching circuit implementation technologies have successfully been studied and used, e.g., in [4], [20], [33]–[37].

The measured relative bandwidth-to-volume ratios (B_r/V) for antenna model 1 and antenna model 2 are presented in Table II. The simulated relative bandwidth-to-volume ratios for the E-GSM900 and GSM1800 reference antennas are $2.1\%/\mathrm{cm}^3$ and $3.6\,\%/\mathrm{cm}^3$, respectively. When the E-GSM900 prototypes are considered, the bandwidth-to-volume ratio of antenna model 1 is over three times as large as that of antenna model 2. When the GSM1800 prototypes are considered, the bandwidth-to-volume ratio of antenna model 1 is about two times as large as that of antenna model 2.

At the E-GSM900 band, the bandwidth-to-volume ratio of antenna model 2 is nearly two times as large as that of the reference antenna. At the GSM1800 band, the bandwidth-to-volume ratio of antenna model 2 is about one third larger than the one of the reference antenna. It should be noted, however, that the shape (see [27]) of the GSM1800 reference antenna element has not been optimized with respect to the bandwidth. Nevertheless, the shape of the GSM1800 reference antenna element can be considered to be rather typical for a single-band internal mobile terminal antenna element. The shape of the E-GSM900 reference antenna element can be considered to be close to optimal with respect to the bandwidth (if the height and location of the antenna element are kept constant).

D. Radiation Patterns

Fig. 4 presents the simulated and measured cuts of the realized gain patterns in free space for the two prototypes of antenna model 1. The realized gain pattern cuts are presented in the standard spherical coordinate system used with antennas. The radial unit is dBi, and the coordinate system is given in Fig. 2. The results include the effect of mismatch loss. The shapes of the realized gain pattern cuts of the prototypes of antenna model 2 were similar to the ones of antenna model 1 and thus, are not presented here.

According to Fig. 4, at 920 MHz the shapes of the realized gain pattern cuts resemble those of a half-wave dipole antenna, which is due to the basic behavior of the antenna structure. As the coupling elements are almost nonradiating at the E-GSM900 frequencies, the thick-dipole type currents of the chassis radiate most of the power.

The measured maximum directivities (D) and maximum realized gains (G_{real}) of the prototype antennas are presented in Table II. The simulated maximum directivities (not shown in Table II) of the E-GSM900 prototype antennas and the E-GSM900 reference PIFA were around 2.2 dBi and therefore, close to the directivity of a lossless dipole antenna (2.15 dBi). The differences between the simulated and measured directivities of the prototype antennas are assumed to be caused by the inaccuracies of the radiation pattern measurement system.

E. Efficiencies in Free Space

Table II presents the measured total and radiation efficiencies (η_{tot} and η_r) for the prototype antennas in free space at the E-GSM900 and GSM1800 system bands. The reported total efficiencies include the losses due to impedance mismatch. The

TABLE III
SIMULATED (SEMCAD) RADIATION EFFICIENCIES AND 10 g AVERAGED SARS FOR ANTENNA MODEL 1, ANTENNA MODEL 2 AND THE REFERENCES ANTENNAS BESIDE THE SAM HEAD MODEL WITH AND WITHOUT THE HAND MODEL. THE CONDUCTIVITIES OF THE METAL PARTS OF THE SIMULATED ANTENNA STRUCTURES HAVE BEEN ASSUMED TO BE INFINITE. THE RESULTS DO NOT INCLUDE THE LOSSES FROM THE MATCHING CIRCUITS OF THE COUPLING ELEMENTS

	900 MHz					
	Antenna model 1		**Antenna model 2**		**Reference antenna**	
Parameter	**head**	**head+hand**	**head**	**head+hand**	**head**	**head+hand**
η_r **[dB]**	-6.8	-7.6	-5.1	-7.4	-4.4	-7.2
$SAR_{10g,head}$ **[W/kg]**	2.0	1.7	1.7	1.4	1.6	1.3
$SAR_{10g,hand}$ **[W/kg]**	-	0.6	-	0.9	-	0.9
	1800 MHz					
	Antenna model 1		**Antenna model 2**		**Reference antenna**	
Parameter	**head**	**head+hand**	**head**	**head+hand**	**head**	**head+hand**
η_r **[dB]**	-3.0	-6.0	-1.9	-4.6	-1.9	-4.4
$SAR_{10g,head}$ **[W/kg]**	0.8	0.7	0.5	0.5	0.4	0.3
$SAR_{10g,hand}$ **[W/kg]**	-	1.0	-	0.9	-	1.4

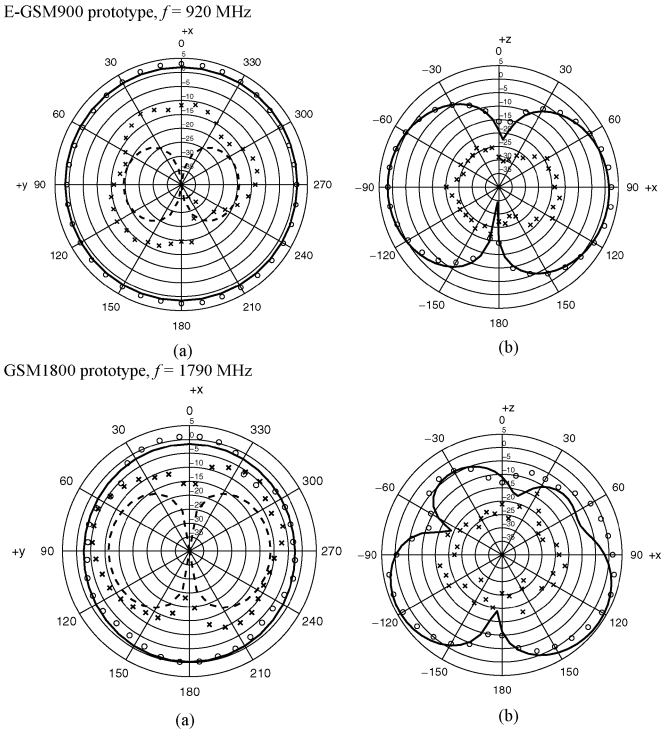

Fig. 4. Simulated (——— E_θ, − − − − E_ϕ) and measured (ooo E_θ, xxx E_ϕ) realized gain pattern cuts for the prototypes of antenna model 1 (a) $\theta = 90°$ and (b) $\phi = 0°$.

simulated (not shown in Table II) radiation efficiencies of the E-GSM900 and GSM1800 prototypes of antenna model 1 were larger than 97% and 96%, respectively. The simulated radiation efficiencies of the E-GSM900 and GSM1800 prototypes of antenna model 2 were larger than 95% and 97%, respectively. Thus, according to Table II, the measured radiation efficiencies of the GSM1800 prototypes are roughly 15% units lower than the simulated ones. The differences between the simulated and measured radiation efficiencies are assumed to be caused by the inaccuracies of the radiation pattern measurement system. Furthermore, according to simulations, the losses caused by the microstrip matching circuits of the prototype antennas are less than 0.15 dB for all prototypes and thus, almost negligible. Nevertheless, the simulated and measured radiation efficiencies are high, and in that respect, the compact antenna structure studied in this paper seems to be suitable for use in mobile terminals.

The simulated free space radiation efficiencies of the reference antennas were larger than 96% and 98% at the E-GSM900 and GSM1800 bands, respectively. Thus, the simulated free space radiation efficiencies of the prototype antennas and the reference antennas are almost identical at both the E-GSM900 and GSM1800 system bands.

F. Efficiencies in Talk-Position

Table III presents for the studied antenna structures the simulated (SEMCAD) radiation efficiencies (η_r) at 900 and 1800 MHz beside the SAM head model with and without the presence of the hand model. For making the comparison of the results easier, the radiation efficiencies are reported in decibels.

1) Efficiencies Without Hand: According to Table III, the radiation efficiency of antenna model 2 at 900 MHz beside the SAM head model is 0.7 dB lower than that of the reference antenna. At 1800 MHz, the radiation efficiencies of antenna model 2 and the reference PIFA are the same. The radiation efficiencies of antenna model 1 beside the SAM head model are notably lower than those of the reference antennas and antenna model 2 at 900 and 1800 MHz. According to [42], SAR maximums in human head tissue can typically be found from locations, where electric field components tangential to the surface of the head tissue are significant. Owing to the shaping and placement of the coupling element of antenna model 1, the tangential electric field components at the surface layer of the head tissue can be expected to be stronger than normally. For this reason most probably, more power is lost to a user's head with antenna model 1 than with traditional designs, in which the antenna elements are placed fully on top of the chassis.

2) Efficiencies With Hand: According to Table III, the simulated radiation efficiencies of antenna model 2 and the reference antennas are almost the same beside the head and hand models at both 900 and 1800 MHz. The losses caused by the hand model are around 2.5 dB for both antenna model 2 and the reference antennas. At 900 MHz, the radiation efficiency of antenna model 1 with the hand model is very close to those of antenna model 2 and the reference antenna. The hand loss of antenna model 1 at 900 MHz is only 0.9 dB, which is considerably less than the hand losses of antenna model 2 and the reference antenna. At

1800 MHz, the hand loss for antenna model 1 is 3 dB. The radiation efficiency of antenna model 1 at 1800 MHz is roughly 1.5 dB lower than those of antenna model 2 and the reference antenna.

G. SARs

Table II presents the measured 10g averaged SARs ($\mathrm{SAR}_{10\ \mathrm{g}}$) and maximum SARs ($\mathrm{SAR}_{\mathrm{max}}$) for the prototype antennas. Table III presents the simulated (SEMCAD) 10 g averaged SARs in the head ($\mathrm{SAR}_{10\ \mathrm{g,head}}$) and hand ($\mathrm{SAR}_{10\ \mathrm{g,hand}}$) models for the studied antenna structures at 900 and 1800 MHz. For each antenna structure, the simulation results obtained with and without the hand model are presented. Considering the uncertainty of the SAR measurements, very good agreement between the simulated and measured SARs can be observed.

1) Measurement Results: For all four prototypes, the measured SAR maximums were located near the middle part of the chassis. For the GSM1800 prototype of antenna model 1, an additional SAR maximum appeared under the coupling element, where the electric field components tangential to the surface of the head model are strong. According to Table II, the measured $\mathrm{SAR}_{10\ \mathrm{g}}$ of antenna model 2 at 900 MHz is clearly lower than that of antenna model 1, as can be expected. For all four prototypes, the measured $\mathrm{SAR}_{10\ \mathrm{g}}$ fall below the European limit for $\mathrm{SAR}_{10\ \mathrm{g}}$ (2 W/kg [43]).

2) Simulations Without Hand: According to Table III, the simulated $\mathrm{SAR}_{10\ \mathrm{g,head}}$ of antenna model 2 without the hand model are close to those of the reference antennas at both 900 and 1800 MHz. The simulated $\mathrm{SAR}_{10\ \mathrm{g,head}}$ of antenna model 1 without the hand model are notably higher than those of antenna model 2 and the reference antennas. The rather high $\mathrm{SAR}_{10\ \mathrm{g,head}}$ of antenna model 1 can be considered to be caused by the same reasons discussed previously. At 900 MHz, the SAR maximums were in all simulated cases located near the middle part of the chassis. At 1800 MHz, an additional local SAR maximum appeared under the coupling element of antenna model 1, similarly as in the measurements. The SAR maximum of the GSM1800 reference antenna appeared under the antenna element. Another weaker SAR maximum was located near the middle part of the chassis. According to [42], peak SAR locations are actually not related to antenna current maximum locations, as has been commonly believed. Instead, SAR maximum locations can be studied by applying electric field boundary conditions to the electric field components perpendicular and parallel to the surface of the head tissue. For example at 900 MHz, the chassis of a mobile terminal creates near-fields similar to those of a dipole antenna. The resulting electric-field components parallel to the surface of the head tissue have a maximum located near the center of the chassis [41], which explains the SAR maximum locations of the studied antenna structures at 900 MHz.

3) Simulations With Hand: According to Table III, the reference antennas have the highest $\mathrm{SAR}_{10\ \mathrm{g,hand}}$ at both 900 and 1800 MHz. At 900 MHz, antenna model 1 has clearly the lowest $\mathrm{SAR}_{10\ \mathrm{g,hand}}$. At 1800 MHz, antenna model 2 has the lowest $\mathrm{SAR}_{10\ \mathrm{g,hand}}$ of the studied antenna structures. In all studied cases, the $\mathrm{SAR}_{10\ \mathrm{g,hand}}$ is lower with the hand model than without the hand model. This is expected [27], since the hand model absorbs some of the power. In general, the SARs of the reference antennas and antenna model 2 beside the head and hand are at the same range at both 900 and 1800 MHz. For all studied antenna structures, the $\mathrm{SAR}_{10\ \mathrm{g,hand}}$ are clearly lower than the specified maximum allowed 4.0 W/kg [43].

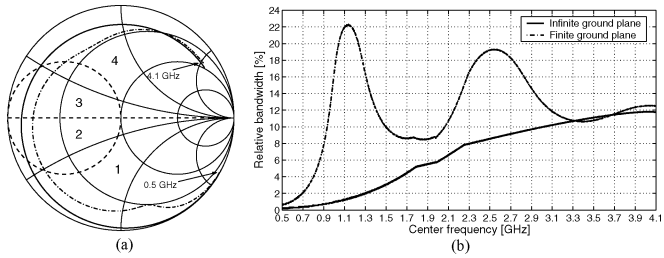

Fig. 5. (a) Smith chart presentation of the simulated (IE3D) input impedance of the coupling element of antenna model 2 with infinite (solid line) and finite ($100\ \mathrm{mm} \times 40\ \mathrm{mm} \times 3\ \mathrm{mm}$, dash-dotted line) ground planes. The thick dashed line separates the four impedance areas (1–4) in which different matching circuit topologies are used. (b) Relative bandwidths ($|S_{11}| \leq -6\ \mathrm{dB}$) obtained when the coupling element of antenna model 2 (with infinite and finite ground planes) is critically matched with single-resonant lossless lumped element matching circuits: 1. Series inductor + parallel inductor 2. Series capacitor + parallel inductor 3. Series inductor + parallel capacitor 4. Series capacitor + parallel capacitor. The lumped element mentioned first is always the component closest to the coupling element.

H. Wideband Simulation Results of Antenna Model 2

According to the simulation and measurement results of the prototype antennas, a single coupling element can be matched at two frequency bands that are rather distant, like, e.g., the E-GSM900 and GSM1800 bands. To further demonstrate the multiband operation of a single coupling element, the input impedance of the coupling element of antenna model 2 was simulated (IE3D) from 0.5–4.1 GHz in 1 MHz steps. Same kind of simulation was also made with the finite ground plane of antenna model 2 replaced with an infinite ground plane. The idea was to examine the effect of the chassis on the radiation behavior of antenna model 2. Using IE3D simulation data, ideal lossless lumped elements were used to match the coupling elements computationally at each simulated frequency point. For each matching point, the frequency responses of the reflection coefficients were calculated and from those, the relative bandwidths ($|S_{11}| \leq -6\ \mathrm{dB}$) were determined. As discussed earlier, the suitable topology for the matching circuitry changes depending on the input impedance of the coupling element at the matching frequency. In consequence, four different kinds of lumped element matching circuit topologies were used. Fig. 5(a) shows Smith chart presentation of the simulated input impedance of the coupling element of antenna model 2 with infinite and finite ($100\ \mathrm{mm} \times 40\ \mathrm{mm} \times 3\ \mathrm{mm}$) ground planes. Also, the four impedance areas, in which different matching circuit topologies are used, are shown. In all cases, the matching was made to 50 Ω, i.e., the antenna structure was critically coupled. Fig. 5(b) presents the obtained relative bandwidths as a function of the matching center frequency.

According to Fig. 5(b), a single coupling element can be matched in very wide frequency range by using different kinds of lumped element matching circuits. The effect of the first, second, and third order resonances of the chassis can clearly be

seen as the bandwidth peaks located at 1.1, 2.5, and 4.0 GHz, respectively. At frequencies less than 3.1 GHz, the contribution of the chassis on the obtained relative bandwidth is significant. For example, at 920 MHz, the relative bandwidth obtained with the finite ground plane is 13 times larger than with the infinite ground plane. At 1800 MHz, the contribution of the chassis on the obtained relative bandwidth is lower than at 920 MHz, as can be expected [19], [21]. The relative bandwidths obtained with the infinite and finite ground planes above 3.1 GHz approach each other because at these frequencies, the studied ground plane dimensions electrically approach infinite ground plane.

VI. Discussion

Using the antenna concept studied in this paper has many advantages and potential applications. The presented results demonstrate that with a simple matching circuit, a single coupling element can be matched at the desired working frequency. As the matching circuitry can be designed separately from the coupling element, the used circuit topology and technology can be chosen flexibly. If coupling elements would be applied on commercial mobile terminals, matching circuitries would most likely be integrated as part of the existing RF front-end module (FOM). Multilayer LTCC substrates commonly used in the FOMs of modern mobile terminals enable the integration of a large number of passive components within a very low substrate volume. Integration of the matching arrangement of the antenna on the FOM also facilitates the implementation of electrically tunable antennas, e.g., for Rx-Tx switching or for frequency agile systems like software or cognitive radios [44]. A multiband antenna can be implemented by simply replacing the single-band matching circuit with a multiband matching circuitry, like in [4]. Moreover, multiresonant matching circuits [4] or other well-known multiresonance techniques used with internal mobile terminal antennas can be applied to enhance the bandwidth of the studied antenna concept.

Current trend in mobile terminal industry is to increase the mechanical complexity of the terminal devices. For example, the so-called flip-phones with built-in cameras, multiple displays, etc., are getting more and more popular. When the mechanics of such a complex phone are changed, e.g., the phone is opened or closed, it is possible that unwanted resonances or other phenomena affecting the matching of the antenna structure appear. In such a case, identification of the sources of these possible problems is extremely important. In traditional internal self-resonant antennas like PIFAs, the matching arrangement is built in to the metallic structure of the antenna element. Therefore, in order to realize multiband antennas, very complex antenna element geometries are typically needed [6]–[10]. Such a complex circuit element, however, can significantly modify the impedance characteristics of, e.g., the possible unwanted resonances. In coupling element-based antenna structures, the matching circuitry is a separate unit from the coupling element. Moreover, even quad-band antenna structures can be implemented with coupling elements having very simple geometries [4]. Therefore, the effects of the mechanics of the phone are typically clearly visible in the input impedance of a coupling element. For example in Fig. 5(a), the chassis resonances can be distinguished clearly from the simulated input impedance of the coupling element (dash-dotted line). Similar information cannot be easily noticed from the input impedance of a PIFA. Identification of the sources of the problems caused by the changing mechanics of the phone, and establishing systematical ways for handling the problems is therefore most likely easier with coupling elements and their matching circuits than with traditional self-resonant antenna solutions. It should be noted, however, that regardless of the used antenna technology, the changes in the mechanics of the phone must still be accounted for.

The presented simulation and measurement results clearly show that compared to traditional internal mobile terminal antenna technologies, significant improvement in terms of relative bandwidth-to-volume ratios can be obtained by using the idea of coupling elements—especially at low frequencies below 1 GHz. For example, the relative bandwidth-to-volume ratio of the E-GSM900 prototype of antenna model 2 was nearly twice as large as that of the E-GSM900 reference antenna. Furthermore, the relative bandwidth-to-volume ratio for the E-GSM900 prototype of antenna model 1 was more than three times as large as that of antenna model 2 and six times as large as that of the E-GSM900 reference antenna. Thus, substantial increase in antenna performance can be obtained by optimally shaping and placing the coupling element at the end of the chassis.

In free space, the simulated radiation efficiencies for all studied antenna structures were almost the same, as can be expected. Typically mobile terminals, however, are held in hand in the standard "cheek" position beside the head of the user [39]. Due to the increasing popularity of multimedia and high data-rate applications, other kinds of use-positions should also be considered in the future. At 900 MHz, the simulated radiation efficiencies with head and hand models were at the same range for all studied antenna structures. The hand loss of antenna model 1 was only 0.9 dB, considerably less than the roughly 2.5 dB hand losses of antenna model 2 and the reference antenna. The very low hand loss of antenna model 1 is possibly just a coincidence. Simulating antenna model 1 with, e.g., different hand locations might give larger average hand loss than 0.9 dB. At 1800 MHz, the simulated radiation efficiency of antenna model 1 with head and hand models was roughly 1.5 dB lower than those of antenna model 2 and the reference antenna. The hand loss of antenna model 1 at 1800 MHz was 3 dB, compared to the roughly 2.5 dB hand losses of antenna model 2 and the reference antenna.

As a general observation, the SAR values in the head and hand models were below the European specifications [43] for all studied antenna structures. At 900 MHz without the hand model, however, the simulated $\mathrm{SAR}_{10\ \mathrm{g,head}}$ of all antenna structures were close to the maximum allowed value of 2 W/kg. One should not, however, further generalize the presented SAR values for commercial mobile terminals. The SAR values of complex commercial mobile terminals and the fully metallic antenna structures studied in this paper are generally not comparable. In [22], a connection between the impedance bandwidths, SARs, and radiation efficiencies of typical PIFA type antenna structures was observed. It was noticed that higher

SAR values and lower radiation efficiencies are obtained when the bandwidth is increased due to stronger excitation of the chassis wavemode. The results of this paper are fully consistent with those of [22]. For example, the $SAR_{10\,g,head}$ of antenna model 1 are generally larger than those of antenna model 2 and the reference PIFAs.

As a summary, coupling elements seem to offer some significant advantages over traditional self-resonant antenna elements. Firstly, it seems that with optimal coupling element shaping and placement, the volume occupied by an internal antenna element can significantly be reduced without decreasing the relative bandwidth. Secondly, very low-profile antenna structures can be implemented for the thin mobile terminals of future. Third, the modularity of the antenna structure should facilitate straightforward implementation of electrically tunable antennas and antennas for mechanically complex mobile terminals. The results of the paper also show a few apparent drawbacks for the studied antenna concept. Since a separate matching circuitry is required, the antenna structure inevitably consumes some space from the FOM substrate. The lumped and distributed components of the matching circuitry obviously also have some effect on the price of the antenna structure. The results further indicate that compared to traditional self-resonant antenna technologies, coupling element-based antenna structures seem to experience somewhat lower radiation efficiencies in the presence of the user. Thus, attention obviously has to be paid on reducing the power absorbed by the head and hand of the user. For commercial mobile terminal manufacturers, the choice between the studied antenna concept and traditional antenna technologies is naturally guided by end-product specifications. An antenna designer eventually needs to prioritize some antenna parameters, and make the decision. The antenna concept studied in this paper seems to be a promising alternative for traditional antenna technologies.

VII. Conclusion

This paper presents a comprehensive study on coupling element based antenna structures for mobile communications terminals. In the first part of the study, design guidelines for the optimum location and shaping of coupling elements in the vicinity of a chassis of the device were identified. Based on the obtained information, two antenna models with different coupling elements were designed and in total four single-band prototypes for the E-GSM900 and GSM1800 systems were constructed. The performances of the prototypes were validated with electromagnetic simulations and measurements both in free space and in the talk-position. In the talk-position, both the effect of the user's head and hand were considered. For comparison, two traditional PIFA-type antenna structures were simulated. The results show that the coupling element based antenna structures are a very potential way of implementing internal mobile terminal antennas. The results of the paper also provide novel and useful information for the future design of low-volume and low-profile antennas for portable terminals.

Acknowledgment

The SAR measurements were performed with equipment co-owned by the Radiation and Nuclear Safety Authority of Finland (STUK) and the Radio Laboratory of Helsinki University of Technology, Espoo, Finland.

References

[1] R. C. Hansen, "Fundamental limitations in antennas," *Proc. IEEE*, vol. 69, no. 2, pp. 170–182, Feb. 1981.

[2] J. McLean, "A re-examination of the fundamental limits on the radiation Q of electrically small antennas," *IEEE Trans. Antennas Propag.*, vol. 44, no. 5, pp. 672–676, May 1996.

[3] R. F. Harrington, "Effect of antenna size on gain, bandwidth, and efficiency," *J. Research Nat. Bureau of Standards*, vol. 64D, pp. 1–12, Jan./Feb. 1960.

[4] J. Villanen, C. Icheln, and P. Vainikainen, "Mobile broadband antennas," in *Proc. XXVIIth URSIGA Conf.*, New Delhi, India, Oct. 2005, BC.2(01464).pdf, on CD-ROM.

[5] J. Ollikainen, O. Kivekäs, A. Toropainen, and P. Vainikainen, "Internal dual-band patch antenna for mobile phones," presented at the AP2000 Millennium Conf. Antennas and Propagation, Davos, Switzerland, Apr. 2000, paper p1111.pdf.

[6] P. Ciais, R. Staraj, G. Kossiavas, and C. Luxey, "Design of an internal quad-band antenna for mobile phones," *IEEE Microw. Wireless Components Lett.*, vol. 14, no. 4, pp. 148–150, Apr. 2004.

[7] M. Martínez-Vázquez and O. Litschke, "Quadband antenna for handeld personal communications devices," in *Proc. IEEE Antennas and Propagation Society Int. Symp.*, Columbus, OH, Jun. 2003, vol. 1, pp. 455–458.

[8] Y.-X. Guo, M. Y. W. Chia, and Z. N. Chen, "Miniature built-in multiband antennas for mobile handsets," *IEEE Trans. Antennas Propag.*, vol. 52, no. 8, pp. 1936–1944, Aug. 2004.

[9] Y.-X. Guo and H. S. Tan, "New compact six-band internal antenna," *IEEE Antennas Wireless Propag. Lett.*, vol. 3, pp. 295–297, 2004.

[10] P. Ciais, R. Staraj, G. Kossiavas, and C. Luxey, "Compact internal multiband antenna for mobile phone and WLAN standards," *Electron. Lett.*, vol. 40, no. 15, pp. 920–921, Jul. 2004.

[11] C. R. Rowell and R. D. Murch, "A capacitively loaded PIFA for compact mobile telephone handsets," *IEEE Trans. Antennas Propag.*, vol. 45, no. 5, pp. 837–842, May 1997.

[12] C. Rowell and R. Murch, "A compact PIFA suitable for dual-frequency 900/1800-MHz operation," *IEEE Trans. Antennas Propag.*, vol. 46, no. 4, pp. 596–598, Apr. 1998.

[13] A. F. Muscat and C. G. Parini, "Novel compact handset antenna," in *Proc. 11th Int. Conf. Antennas and Propagation*, Manchester, U.K., Apr. 2001, vol. 1, pp. 336–339.

[14] W. S. Chen, T. W. Chiou, and K. L. Wong, "Compact PIFA for GSM/DCS/PCS triple-band mobile phone," in *Proc. IEEE Antennas and Propagation Society Int. Symp.*, San Antonio, TX, Jun. 2002, vol. 4, pp. 528–531.

[15] S. Tarvas and A. Isohätälä, "An internal dual-band mobile phone antenna," in *IEEE Antennas and Propagation Society Int. Symp.*, Salt Lake City, UT, Jul. 2000, vol. 1, pp. 266–269.

[16] O. Kivekäs, J. Ollikainen, and P. Vainikainen, "Wideband dielectric resonator antenna for mobile phones," *Microw. Op. Technol. Lett.*, vol. 36, no. 1, pp. 25–26, Jan. 2003.

[17] K. Kawahata, A. Miyata, and Y. Ishikawa, "A miniaturized dielectric ceramic resonator antenna for mobile handset application," presented at the XXVIIth General Assembly of the Int. Union of Radio Science, Maastricht, The Netherlands, Aug. 2002, paper p1092.pdf.

[18] S. Nagumo, K. Kawahata, Y. Saitoh, M. Ida, and Y. Ishikawa, "Dual resonance chip dielectric antenna with a slant gap for handheld wireless communication tools," presented at the AP2000 Millennium Conf. Antennas and Propagation, Davos, Switzerland, Apr. 2000, paper p0591.pdf.

[19] P. Vainikainen, J. Ollikainen, O. Kivekäs, and I. Kelander, "Performance analysis of small antennas mounted on mobile handsets," in *Proc. COST 259 Final Workshop—The Mobile Terminal and Human Body Interaction*, Bergen, Norway, Apr. 26–27, 2000, p. 8.

[20] P. Vainikainen, J. Ollikainen, O. Kivekäs, and I. Kelander, "Modular Coupling Structure for a Radio Device and a Portable Radio Device," Finland Pat. FI114260, Appl. 20002529, 17.11.2000, (15.09.2004) 22 p..

[21] P. Vainikainen, J. Ollikainen, O. Kivekäs, and I. Kelander, "Resonator-based analysis of the combination of mobile handset antenna and chassis," *IEEE Trans. Antennas Propag.*, vol. 50, no. 10, pp. 1433–1444, Oct. 2002.

[22] O. Kivekäs, J. Ollikainen, T. Lehtiniemi, and P. Vainikainen, "Bandwidth, SAR, and efficiency of internal mobile phone antennas," *IEEE Trans. Electromagn. Compat.*, vol. 46, no. 1, pp. 71–86, Feb. 2004.
[23] D. Manteuffel, A. Bahr, and I. Wolff, "Investigation on integrated antennas for GSM mobile phones," presented at the AP2000 Millennium Conf. Antennas and Propagation, Davos, Switzerland, Apr. 2000, paper p0351.pdf.
[24] R. Yamaguchi, K. Sawaya, Y. Fujino, and S. Adachi, "Effect of dimensions of conducting box on radiation pattern of a monopole antenna for portable telephone," *IEICE Trans. Commun.*, vol. E-76-B, no. 12, pp. 1526–1531, Dec. 1993.
[25] K. Boyle, "Radiating and balanced mode analysis of PIFA shorting pins," in *IEEE Antennas and Propagation Society Int. Symp.*, San Antonio, Texas, Jun. 2002, vol. 4, pp. 508–511.
[26] A. T. Arkko and E. A. Lehtola, "Simulated impedance bandwidths, gains, radiation patterns and SAR values of a helical and a PIFA antenna on top of different chassiss," in *Proc. 11th Int. Conf. Antennas and Propagation*, Manchester, U.K., Apr. 2001, pp. 651–654.
[27] K. Sato, K. Matsumoto, K. Fujimoto, and K. Hirasawa, "Characteristics of a planar inverted-F antenna on a rectangular conducting body," *Electron. Commun. Jpn.*, vol. 72, no. 10, pp. 43–51, 1989.
[28] R. F. Harrington and J. R. Mautz, "Theory of characteristic modes for conducting bodies," *IEEE Trans. Antennas Propag.*, vol. 19, no. 5, pp. 622–628, Sep. 1971.
[29] R. J. Garbacz and R. H. Turpin, "A generalized expansion for radiated and scattered fields," *IEEE Trans. Antennas Propag.*, vol. 19, no. 3, pp. 348–358, May 1971.
[30] E. Antonino-Daviu, M. Cabedo-Fabres, M. Ferraro-Bataller, and J. I. Herranz-Herruzo, "Analysis of the coupled chassis-antenna modes in mobile handsets," presented at the IEEE Antennas and Propagation Society Int. Symp., Monterey, CA, Jun. 2004, paper S098p02a.pdf.
[31] K. Boyle and , Koninklijke Philips Electronics N.V., "Antenna Arrangement," The Netherlands Pat. US6674411 B2, Appl. 10/085696, 27.02.2002, (06.01.2004), 6 p..
[32] G. Matthaei, L. Young, and E. M. T. Jones, *Microwave Filters, Impedance-Matching Networks, and Coupling Structures*. New York: Mc Graw-Hill, 1964, p. 1095.
[33] Press releases, "World's smallest GSM front-end module," EPCOS AG. Munich, Germany, Aug. 2001 [Online]. Available: http://www.epcos.com/
[34] Press releases, "GSM modules: world's smallest FEM," EPCOS AG. Munich, Germany, Nov. 2004 [Online]. Available: http://www.epcos.com/
[35] O.-S. Lin, C.-C. Liu, K.-M. Li, and C. H. Chen, "Design of an LTCC triband transceiver module for QPRS mobile applications," *IEEE Trans. Microwave Theory Tech.*, vol. 52, no. 12, pp. 2718–2724, Dec. 2004.
[36] L. K. Yeung and K.-L. Wu, "A compact second-order LTCC bandpass filter with two finite transmission zeros," *IEEE Trans. Microw. Theory Tech.*, vol. 51, no. 2, pp. 337–341, Feb. 2003.
[37] A. Sutono, D. Heo, Y.-J. E. Chen, and J. Laskar, "High-Q LTCC-based passive library for wireless system-on-package (SOP) module development," *IEEE Trans. Microw. Theory Tech.*, vol. 49, no. 10, pp. 1715–1724, Oct. 2001.
[38] H. Arai, *Measurement of Mobile Antenna Systems*. Boston, MA: Artech House, 2001, pp. 56–57.
[39] *Basic Standard for the Measurement of Specific Absorption Rate Related to Human Exposure to Electromagnetic Fields From Mobile Phones (300 MHz–3 GHz)*, European standard EN 50361, CENELEC, Jul. 2001, Brussels, Belgium, 51 p..
[40] DASY4, Dosimetric Assessment System for SAR Measurements Schmid & Partner Engineering AG (SPEAG). Zurich, Switzerland [Online]. Available: http://www.dasy4.com/welcome.html/
[41] SEMCAD, a Finite-Difference Time-Domain (FDTD) Based 3D Full-Wave Electromagnetic Solver for SAR Simulations Schmid & Partner Engineering AG (SPEAG). Zurich, Switzerland [Online]. Available: http://www.semcad.com/news.html/
[42] O. Kivekäs, T. Lehtiniemi, and P. Vainikainen, "On the general energy-absorption mechanism in the human tissue," *Microw. Opt. Technol. Lett.*, vol. 43, no. 3, pp. 195–201, Nov. 2004.
[43] The Council of the European Union, "Council recommendation on 12 July 1999 on the limitation of exposure of the general public to electromagnetic fields (0 Hz to 300 GHz)," *Official J. Eur. Communities*, pp. 59–70, Jul. 1999, 1999/519/EC, L 199.
[44] J. Mitola and G. Q. Maquire, "Cognitive radio: making software radios more personal," *IEEE Personal Commun.*, vol. 6, no. 2, pp. 13–18, Aug. 1999.
[45] H. W. Fano, "Theoretical limitations on the broadband matching of arbitrary impedances," *J. Franklin Institute*, vol. 249, no. 1, pp. 57–83, Jan. 1950, and No. 2, Feb. 1950, pp. 139 154.
[46] IE3D, a Moment-Method (MoM) Based Commercial Simulator ver. 10.0, Zeland software inc. Fremont, USA [Online]. Available: http://www.zeland.com/

Juha Villanen was born in Helsinki, Finland, 1979. He received the M.Sc. degree in electrical engineering from Helsinki University of Technology (TKK), Espoo, Finland, in 2003, where he is currently working toward the Doctorate degree.

Since 2002, he has worked as a Research Engineer at the Radio Laboratory of TKK. His research interests include design and implementation techniques of low-volume mobile terminal antennas, especially coupling elements based antenna structures.

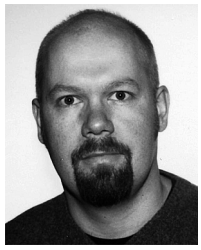

Jani Ollikainen (M'03) was born in Lahti, Finland, in 1971. He received the Master of Science in Technology, Licentiate of Science in Technology, and Doctor of Science in Technology degrees in electrical and communications engineering from Helsinki University of Technology (TKK), Espoo, Finland, in 1997, 2000, and 2004, respectively, .

From 1996 until 2003, he worked as a Researcher at the Radio Laboratory of TKK. In early 2003, he joined Nokia Research Center in Helsinki, Finland, where he is currently working as a Research Manager. His research interests include design, implementation, and measurement techniques of small antennas for personal mobile communications.

Outi Kivekäs was born in Helsinki, Finland. She received the Master of Science in Technology, Licentiate of Science in Technology, and Doctor of Science in Technology degrees in electrical engineering from Helsinki University of Technology (TKK), Espoo, Finland, in 1999, 2001, and 2005, respectively.

From 1998 to 2005, she worked as a Research Engineer at the Radio Laboratory, TKK. Her research interests include mobile terminal antennas and their user interaction.

Pertti Vainikainen (M'91) received the Master of Science in Technology, Licentiate of Science in Technology, and Doctor of Science in Technology degree from Helsinki University of Technology (TKK), Espoo, Finland, in 1982, 1989, and 1991, respectively.

From 1992 to 1993, he was an Acting Professor of radio engineering, in 1993, he was an Associate Professor of radio engineering, and since 1998, he has been a Professor in radio engineering, all in the Radio Laboratory of TKK. From 1993 to 1997, he was the Director of the Institute of Radio Communications (IRC) of TKK, and in 2000, a Visiting Professor at Aalborg University, Denmark. He is the author or coauthor of six books and about 240 refereed international journal or conference publications and the holder of seven patents. His main fields of interest are antennas and propagation in radio communications and industrial measurement applications of radio waves.